

Size, shade or shape? The contribution of galaxies of different types to the star-formation history of the Universe from *SDSS-IV MaNGA*

Thomas Peterken,^{1*} Alfonso Aragón-Salamanca,^{1†} Michael Merrifield,¹
 Vladimir Avila-Reese,² Nicholas F. Boardman,³ Helena Domínguez Sánchez,⁴
 Dmitry Bizyaev,⁵ Niv Drory,⁶ Kaike Pan,⁵ Joel R. Brownstein⁷

¹*School of Physics and Astronomy, University of Nottingham, University Park, Nottingham NG7 2RD, UK*

²*Instituto de Astronomía, Universidad Nacional Autónoma de México, A.P. 70–264, 04510 CDMX, México*

³*Department of Physics and Astronomy, University of Utah, Salt Lake City, UT 84112, USA*

⁴*Institute of Space Sciences (ICE, CSIC), Campus UAB, Carrer de Magrans, E-08193 Barcelona, Spain*

⁵*New Mexico State University, Apache Point Observatory, P.O. Box 59, Sunspot, NM 88349*

⁶*McDonald Observatory, The University of Texas at Austin, 1 University Station, Austin, TX 78712, USA*

⁷*Department of Physics and Astronomy, University of Utah, 115 S. 1400 E., Salt Lake City, UT 84112, USA*

Draft copy: 29 January 2021

ABSTRACT

By fitting stellar populations to SDSS-IV MaNGA survey observations of ~ 7000 suitably-weighted individual galaxies, we reconstruct the star-formation history of the Universe, which we find to be in reasonable agreement with previous studies. Dividing the galaxies by their present-day stellar mass, we demonstrate the downsizing phenomenon, whereby the more massive galaxies hosted the most star-formation at earlier times. Further dividing the galaxy sample by colour and morphology, we find that a galaxy’s present-day colour tell us more about its historical contribution to the cosmic star formation history than its current morphology. We show that downsizing effects are greatest among galaxies currently in the blue cloud, but that the level of downsizing in galaxies of different morphologies depends quite sensitively on the morphological classification used, due largely to the difficulty in classifying the smaller low-mass galaxies from their ground-based images. Nevertheless, we find agreement that among galaxies with stellar masses $M_{\star} > 6 \times 10^9 M_{\odot}$, downsizing is most significant in spirals. However, there are complicating factors. For example, for more massive galaxies, we find that colour and morphology are predictors of the past star formation over a longer timescale than in less massive systems. Presumably this effect is reflecting the longer period of evolution required to alter these larger galaxies’ physical properties, but shows that conclusions based on any single property don’t tell the full story.

Key words: galaxies: evolution

1 INTRODUCTION

The question of when and where the stars residing in today’s galaxies formed is essential to understanding the present-day Universe. Since early works by Madau et al. (1996), Connolly et al. (1997) and others, many studies have measured the average instantaneous star-formation rate in galaxy populations observed at different redshift snapshots to build a picture of the overall cosmic star-formation history; see Madau & Dickinson 2014 for a comprehensive review. These approaches have built up a picture of a two-phase star-formation history of the Universe, with the mean star-formation rate per unit of comoving volume rising rapidly during the first 1–2 Gyr

(i.e. $z > 4$) after the Big Bang, and declining in more recent times. The exact lookback time at which the peak of cosmic star-formation occurred is uncertain, but most sources agree that it is broadly in the range of $z = 1 - 3$, corresponding to approximately 8–11 Gyr before the present day; see analyses by Hopkins & Beacom (2006), Behroozi et al. (2013), and Madau & Dickinson (2014), and references therein.

Within this picture, studies of galaxy populations at different redshifts have demonstrated the link between the star-formation history of the Universe and the evolution of its constituent galaxies. For example, many show that the star-formation rate of galaxies with high stellar mass peaked and declined at preferentially earlier times than low-mass galaxies (Cowie et al. 1996; Fontanot et al. 2009; Peng et al. 2010; Muzzin et al. 2013), an effect normally referred to as “downsizing”. Others have proven that a link between a galaxy’s

* E-mail: Thomas.Peterken@nottingham.ac.uk

† E-mail: Alfonso.Aragon@nottingham.ac.uk

morphology and its contribution to the cosmic star-formation history exists over a range of redshifts (Wuyts et al. 2011; Bell et al. 2012; Cheung et al. 2012; Mortlock et al. 2013; Moresco et al. 2013), although determining detailed morphologies at high redshift is of course difficult.

It has long been known that in the present-day Universe, spirals are generally bluer in colour (e.g. Holmberg 1958) due to their higher rate of star formation (e.g. Roberts 1963; Kennicutt 1983), and are less massive (Blanton & Moustakas 2009) than earlier-type galaxies, suggesting an evolutionary sequence of galaxies transitioning from late to early types as they grow and subsequently cease their star-formation. However, the exact mechanisms by which galaxies are able to alter their shape and colour are still not fully understood. One avenue to studying the typical evolution processes which have occurred in galaxies could be to determine whether a present-day galaxy’s colour¹ or its morphology is the strongest indicator to its past. It would then be possible to understand which property transition — morphology or colour; “shape” or “shade” — is more fundamental, and whether the associated timescales vary according to galaxy properties such as stellar mass.

Unfortunately, by their nature, studies of galaxy populations at different redshifts are limited to studying the average statistical behaviour of a galaxy population’s star-formation at different snapshots in the Universe’s history, and are therefore unable to trace how individual galaxies have evolved. In order to understand the link between a galaxy’s *present-day* properties and its past contribution to the cosmic star-formation history, an alternative approach is therefore required.

Using large samples of galaxies from spectroscopic surveys, Panter et al. (2003, 2007) and Heavens et al. (2004) showed that by measuring galaxies’ individual star-formation histories using spectral fitting techniques, the star-formation history of the Universe can be reconstructed. Despite significant progress in more recent years, obtaining accurate non-parametric star-formation histories of galaxies in this manner is still subject to significant uncertainties, particularly those due to difficulties in creating reliable stellar population templates using stellar evolution models which are still poorly understood (Charlot et al. 1996; Maraston 1998, 2005; Yi 2003; Lee et al. 2007; Ge et al. 2019), and also due to assumptions about the behaviour of the stellar initial mass function (Maraston 1998; van Dokkum et al. 2008; Pforr et al. 2012; Cid Fernandes et al. 2014) and the treatment of stellar elemental abundances. See Conroy et al. (2009, 2010), and Conroy & Gunn (2010) for a set of detailed reviews and discussion on this important subject.

However, notwithstanding these difficulties, many studies have shown that non-parametric stellar population fitting methods produce generally reliable results (see e.g. Cid Fernandes et al. 2005; Panter et al. 2007; Sánchez et al. 2016; Li et al. 2017; de Amorim et al. 2017; Ge et al. 2018; Cid Fernandes 2018; see also Appendix A of Peterken et al. 2020 for tests specific for the spectral fitting methods used here), and these stellar population “fossil record” methods have therefore been successfully applied to modern integral-field spectroscopic galaxy surveys to uncover the history of low-redshift galaxies and their physical components (see e.g. Cid Fernandes et al. 2013; Pérez et al. 2013; Ibarra-Medel et al. 2016; González Delgado et al. 2016, 2017; Peterken et al. 2019, 2020; García-Benito et al. 2019; Fraser-McKelvie et al. 2019). Others have used spectral fitting analyses to show that a galaxy’s observed colour (e.g. Ibarra-

Medel et al. 2016; or equivalently star-formation rate, e.g. Sánchez et al. 2019) and morphology (e.g. García-Benito et al. 2017; López Fernández et al. 2018; Lacerna et al. 2020; Bellstedt et al. 2020) are directly linked to the historical evolution of its star formation rate. In a cosmological context, López Fernández et al. (2018) and Sánchez et al. (2019) have demonstrated the power of using fossil record techniques to reconstruct how galaxies’ physical properties have evolved over cosmic time, showing good agreement with redshift snapshot studies, and thereby justifying this approach as a complementary analysis technique to study the connection between the Universe’s evolution with its present-day galaxies.

With its consistent radial coverage of a large sample of galaxies with varying physical properties, the integral-field spectroscopic MaNGA survey (Bundy et al. 2015) (part of the fourth generation of the Sloan Digital Sky Survey; SDSS-IV; Blanton et al. 2017) offers an ideal tool to investigate the link between today’s galaxies and the Universe’s past. In Peterken et al. (2021), we explored how the stellar population fossil record can reveal the cosmic evolution of the star-formation “main sequence” and the mass function of galaxies. Here, we use the same measured star-formation histories of a large sample of galaxies to derive the star-formation history of the Universe, and make use of morphological information from both citizen science and machine learning classifications to explore the connection between present-day stellar mass, colour, and morphology to a galaxy’s star-formation rate evolution over the age of the Universe.

This paper is structured as follows. In Section 2, we outline the relevant details of the SDSS-IV MaNGA survey. We outline how the samples were selected and describe the division of these samples into morphological and colour sub-samples in Section 3. We then briefly summarise the spectral fitting methods we employ to measure galaxy star-formation histories in Section 4. Section 5 contains the derivation of the cosmic star-formation history and its contribution from galaxies of different present-day stellar masses (5.1), colour (5.2), and morphological classifications (5.3). Finally, we interpret how these results fit into a context of downsizing and discuss the relative importance of morphology and broadband colour in Section 6.

Throughout this paper, we assume a flat Λ CDM cosmology with $H_0 = 68 \text{ km s}^{-1} \text{ Mpc}^{-1}$ and $\Omega_m = 0.308$, consistent with Planck Collaboration et al. (2016).

2 MANGA

As part of the SDSS-IV, Mapping Nearby Galaxies at Apache Point Observatory (MaNGA; Bundy et al. 2015) is an integral-field spectroscopic galaxy survey. As of the time of writing, on-site operations have been completed, and by the end of 2020 the fully-reduced observations will be available for over 10,000 low-redshift ($0.01 < z < 0.15$, median $z \sim 0.3$) galaxies with a spatial resolution of 2.5 arcseconds (Yan et al. 2016b). Observations make use of specially-designed integral field units of five sizes ranging from 12 to 32 arcsecond diameters with 19 to 127 fibres (Drory et al. 2015), which are mounted onto plates on the 2.5-metre Sloan telescope at Apache Point Observatory in New Mexico (Gunn et al. 2006). The fibres are fed into the BOSS spectrographs (Smee et al. 2013) and the spectra are calibrated to better than 5% accuracy (Yan et al. 2016a) covering a wavelength range of 3600 – 10300 Å with a resolution of $R \approx 2000$. Observations are designed to reach a minimum

¹ “Colour” here refers to a broadband measure of the spectral energy distribution in the optical region

signal-to-noise ratio of 5 \AA^{-1} at $1.5 R_e$ (Law et al. 2015), where R_e is the effective radius of each observed galaxy measured by the NASA-Sloan Atlas (NSA; Blanton et al. 2011).

The calibrated spectra are reduced and combined into three-dimensional datacubes by a custom data reduction pipeline (DRP; Law et al. 2016; Law et al. in preparation), and a data analysis pipeline (DAP; Westfall et al. 2019; Cherinka et al. 2019) provides data analysis products such as spectral index maps, stellar and gas kinematics, and emission line fluxes (Belfiore et al. 2019).

3 SAMPLE SELECTION

MaNGA targets galaxies with a flat distribution in $\log(\text{stellar mass})$ over the range of $10^9 M_\odot < M_\star < 10^{11.5} M_\odot$, and the full targeting catalogue assigns galaxies to designated samples. The Primary sample galaxies are observed to a radius of $1.5 R_e$, while the Secondary sample contains observations to $2.5 R_e$. The Primary sample is supplemented by a colour-enhanced sample to form the Primary+ sample, which over-samples unusual regions of the stellar mass–colour plane such as high-mass blue galaxies, low-mass red galaxies, and the “green valley” (Law et al. 2015).

From the latest internal MaNGA data release (MaNGA Product Launch 9; MPL-9), we selected all galaxies belonging to any of the Primary, Primary+, or Secondary samples. In doing so, we required the MaNGA DRP to have assigned no warning flags at all to any galaxy (i.e. `drp3qua1=0` for all galaxies). We also require the DAP to have successfully modelled an emission spectrum cube for each galaxy. These criteria produce a full sample of 6861 galaxies, of which 3255 belong to the Primary sample, 4342 to the Primary+ sample, and 2519 to the larger-coverage Secondary sample.

3.1 Sample weightings

As a result of MaNGA’s sampling, none of the survey’s galaxy samples are intrinsically volume-limited. However, since the sampling strategies are well-defined, each galaxy can be assigned an appropriate weighting such that any analysis can be performed on an effectively volume-limited sample (Wake et al. 2017). An implementation of these weightings is described in detail by Wake et al. (2017), but here — as in Peterken et al. (2021) — we use weightings generated using the method implemented by Sánchez et al. (2019); see also Rodríguez-Puebla et al. (2020) and Calette et al. (in preparation) for further details. This choice of which set of weightings to use was due to the Sánchez et al. (2019) weightings being more robust at lower stellar masses and more detailed in its treatment of galaxy colour. However, since the sample-weighting calculations are similar, we find that the results shown here are unchanged when the Wake et al. (2017) sample weightings are used instead. The adopted galaxy weights are reliable for galaxies with stellar mass $M_\star > 10^9 M_\odot$, making this the limit above which each of the properly-weighted samples are effectively volume-limited.

3.2 Comparison to single-fibre spectra

The weighted distributions of angular radii for each of the samples is shown in Figure 1. For each of the samples, the majority of galaxies’ $1.2 R_e$ radius threshold (as used in this work; see Section 4) is larger than the 3 arcsec radius probed by single-fibre SDSS spectra, highlighting the extra information available with integral-field spectroscopic observations. As well as including more of the total

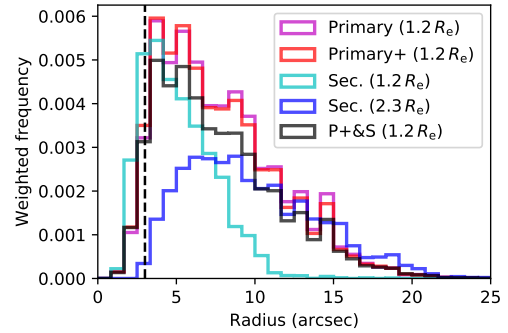


Figure 1. The weighted distributions of galaxy radii. Each galaxy is sampled to $1.2 R_e$ (and $2.3 R_e$ for Secondary-sample galaxies), resulting in a distribution of on-sky apertures. All samples probe to larger angular apparent radii than SDSS single-fibre spectra (marked as a vertical dashed line) would.

star-formation in the Universe, the spectra we use here are measuring consistent radii in all galaxies regardless of their observed redshift.

4 SPECTRAL FITTING

In Peterken et al. (2021), we describe how we implemented full-spectrum fitting techniques to each Primary+ galaxy. We use an identical method here but also including galaxies in the Secondary sample. To summarise; we removed emission lines from each spaxel using the DAP’s emission-line spectrum, and combined all spaxels’ spectra within $1.2 R_e$ of each galaxy after removing line-of-sight velocities. We then fit a single spectrum of the stellar component for each galaxy using STARLIGHT, with a combination of 54 single stellar population (SSP) spectra from the E-MILES (Vazdekis et al. 2016) and Asa’d et al. (2017) libraries as templates. We also assume a Calzetti et al. (2000) dust extinction model and fit within the range $3541.4 \leq \lambda \leq 8950.4 \text{ \AA}$. Typical combined signal-to-noise ratios for each galaxy within the fitting range are at least ~ 500 . Further description of the fitting method can be found in Peterken et al. (2021), and we also refer the reader to Peterken et al. (2020) for a full assessment of its reliability.

As well as fitting the spectrum of each galaxy sampled to $1.2 R_e$, we also repeat the above fitting method using all spaxels of all Secondary galaxies sampled to $2.3 R_e$. We therefore obtained 9380 individual fits; one of each Primary+ galaxy, and two for each Secondary galaxy (sampled to each radius limit). The two aperture limits were chosen to balance the inclusion of as much of the MaNGA field of view as possible, while avoiding overlap with the hexagonal IFU edges which might contaminate and bias results (see e.g. Ibarra-Medel et al. 2016).

We then obtain a 0.2 dex time-smoothed star-formation history of each of the fits using the SSP weights assigned by STARLIGHT using the method described in Peterken et al. (2021). In smoothing, the STARLIGHT-derived star-formation history (in units of $M_\odot \text{ yr}^{-1}$) is first resampled at 250 lookback times which are evenly spaced in $\log(\text{time})$ over the range of stellar populations used in fitting, and then convolved in the $\log(\text{time})$ axis with a Gaussian function of width 0.2 dex.

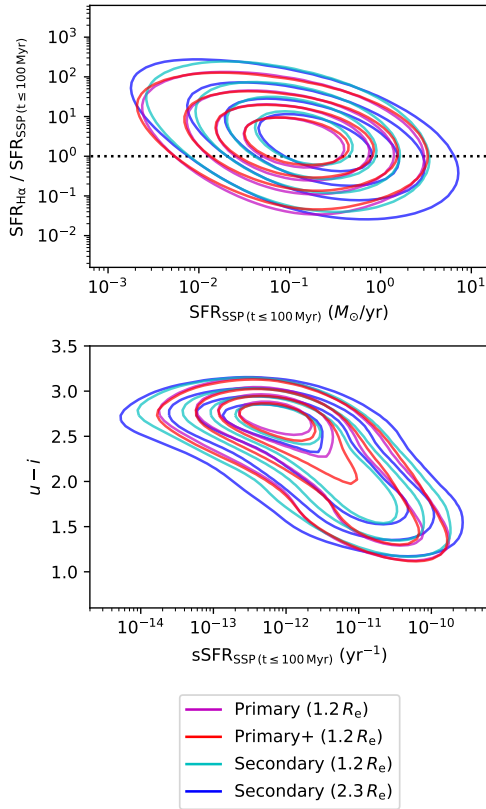


Figure 2. The present-day star-formation rates measured using both $H\alpha$ emission $SFR_{H\alpha}$ are consistent with STARLIGHT-derived total star-formation rate over the last 100 Myr $SFR_{SSP, (t \leq 100 \text{ Myr})}$ (top). The NSA $u - i$ broadband colours are also closely linked to the present-day specific star formation rate (bottom). Coloured contours indicate lines of 20%, 40%, 60%, and 80% of the peak density for each of the *unweighted* samples.

4.1 Comparison of measured star-formation rates

To establish the trustworthiness of the spectral fitting methods, we compare the measured outputs with known results obtained through established analyses. We find that the total stellar mass measurements for each galaxy agree well with those determined photometrically by the NASA-Sloan Atlas (see Peterken et al. 2020).

We are also able to compare the present-day star-formation rates of each galaxy measured using the STARLIGHT-derived star-formation histories with those calculated entirely independently from $H\alpha$ fluxes. For each galaxy, we corrected the DAP’s map of Gaussian-modelled $H\alpha$ emission line flux using the Balmer decrement, assuming an intrinsic value of $f_{H\alpha}/f_{H\beta} = 2.87$ (corresponding to electron temperature $T_e = 10^4$ K and density $n_e = 10^2 \text{ cm}^{-3}$ under Osterbrock & Ferland (2006) “Case B” recombination) and a Calzetti et al. (2000) reddening curve with $R_V = 3.1$. Note that in the stellar population modelling in Section 4, we assume $R_V = 4.05$, but the lower value is used when considering the emission lines; see Catalán-Torrecilla et al. (2015) and Greener et al. (2020) for an explanation on the difference between dust corrections applied to stellar and gas spectra. These calculations and corrections are detailed fully by Greener et al. (2020).

We then summed the flux from all spaxels within $1.2 R_e$ (and $2.3 R_e$ for the Secondary sample) which have an emission-line signal-to-noise ratio of at least 10 and calculated the star-formation rate $SFR_{H\alpha}$ using the relation described by Kennicutt (1998). For

consistency with the SSP templates used in fitting with STARLIGHT, we assume a Chabrier (2003) IMF for this calculation.

We also calculate a present-day star-formation rate from STARLIGHT $SFR_{SSP, (t \leq 100 \text{ Myr})}$ by extracting from the smoothed star-formation histories the total mass added to each galaxy over the last 100 Myr. By plotting the offset between $SFR_{H\alpha}$ and $SFR_{SSP, (t \leq 100 \text{ Myr})}$ as a function of $SFR_{SSP, (t \leq 100 \text{ Myr})}$, we show in Figure 2 that these two measurements of the ongoing star-formation rate are broadly comparable despite the $H\alpha$ emission having been removed from the spectra prior to fitting. The offset from the line of equality is to be expected given that the two measurements are using completely different approaches and calibrations, contain differing systematics, and are sensitive to different timescales of star-formation. For the Primary+ sample, we find that the relationship between the two measurements can be described by

$$\log\left(\frac{SFR_{H\alpha}}{SFR_{SSP, (t \leq 100 \text{ Myr})}}\right) = -0.5 \log\left(SFR_{SSP, (t \leq 100 \text{ Myr})}\right) - 0.1 \quad (1)$$

with a root mean square deviation of ~ 0.7 dex from this best-fit line. Comparable relationships are found for the other samples. The relatively small offset does not affect any conclusions, reassuring that the stellar population fits are reliable.

We obtain STARLIGHT-derived specific star-formation rates $sSFR_{SSP, (t \leq 100 \text{ Myr})}$ by calculating the ratio of $SFR_{SSP, (t \leq 100 \text{ Myr})}$ to the total STARLIGHT-measured stellar mass contained within each present day galaxy. We also show in Figure 2 that such specific star-formation rates are closely correlated with a galaxy’s $u - i$ NSA broadband colour, with a best-fit relation in the Primary+ sample described by

$$u - i = -0.3 \log\left(SFR_{SSP, (t \leq 100 \text{ Myr})}\right) - 1.7 \quad (2)$$

which has a root mean square deviation of ~ 0.4 mag. As before, comparable relationships also exist for the other galaxy samples. This link is unsurprising, as the redder i band is most sensitive to the low-mass stars which comprise the bulk of a galaxy’s total stellar mass, while the u band is more sensitive to bluer stars and is therefore indicative of recent star-formation, making $u - i$ a suitable proxy for specific star-formation rate.

5 THE STAR-FORMATION HISTORY OF THE UNIVERSE

Having obtained individual star-formation histories for each galaxy, the cosmic star-formation history can be constructed. To do so, the individual star-formation histories measured for each galaxy must be carefully weighted and combined. In combining galaxy star-formation histories, we account for the lookback time due to the observed redshift of each galaxy. Each star-formation history’s age sampling is shifted onto a lookback-time sampling by adding the galaxy’s redshift’s lookback time. The galaxy star-formation histories are then combined and interpolated onto a common sampling of lookback times.

Since the Primary(+) and Secondary samples are selected from different redshift distributions (Wake et al. 2017) — as shown in Figure 3 — any derived star-formation history of the Universe will only be able to probe down to a specific limit in lookback times, depending on which sample is used. Since the distribution of galaxy redshifts within any sample is dependent on the galaxy mass, we only

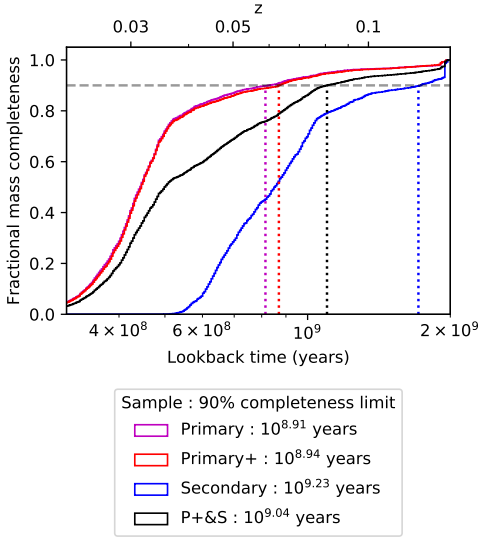


Figure 3. Fractional cumulative completeness in sample-weighted stellar mass as a function of lookback time, due to galaxies’ observed redshifts. The Secondary sample contains galaxies at higher redshifts than the Primary and Primary+ samples. The lookback times corresponding to a 90% mass completeness for each sample are given in the legend, and are illustrated by vertical dotted lines. We do not sample star-formation histories at lookback times below these limits.

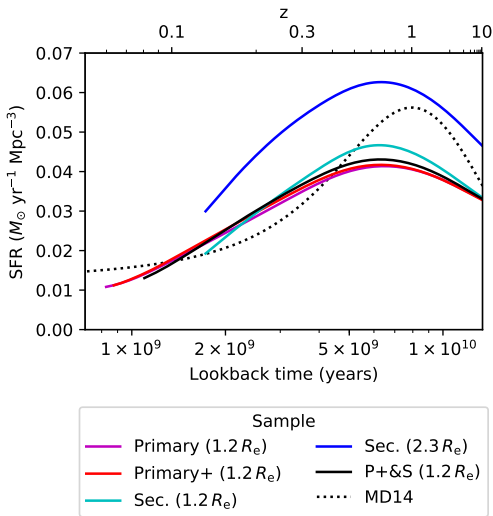


Figure 4. The star-formation history of the Universe determined using the different galaxy samples (solid coloured lines). The agreement between the Primary and Primary+ samples is too close to be able to properly distinguish between them. Also shown is the [Madau & Dickinson \(2014\)](#) best-fit parametric function to the cosmic star-formation history derived from galaxy redshift studies (black dotted line). For consistency, this comparison study has been smoothed according to our treatment of each individual galaxy’s star-formation history.

measure cosmic star-formation histories at lookback times greater than that for which each sample has at least 90% completeness in sample-weighted mass. The specific adopted limits are shown in Figure 3.

The cosmic star-formation histories measured from each sample is shown for each sample in Figure 4. We show that the calculated

star-formation history of the Universe measured within $1.2 R_e$ of each galaxy agrees well at all lookback times regardless of the MaNGA sample used, and that all samples show a peak cosmic star-formation history at a lookback time of $10^{9.80 \pm 0.01}$ years (corresponding to $z \approx 0.67 \pm 0.02$).

Figure 4 also shows the best-fit function derived by [Madau & Dickinson \(2014\)](#) of the cosmic star-formation history measured through galaxy redshift studies. To ensure a like-for-like comparison, we calculated the mass weights which would be assigned to each SSP template age used in our fitting method based on Equation 15 of [Madau & Dickinson \(2014\)](#), by integrating the curve within a box centred in log-space on each SSP’s nominal age, to obtain a raw star-formation history as might ideally be measured using the stellar population fitting methods described in Section 4. We then smoothed the modelled SSP weights using the procedure described in Section 4 and in [Peterken et al. \(2021\)](#). This smoothing procedure results in the smoothed profile showing a broader peak in the cosmic star-formation history which occurs at a lower redshift (at $z \sim 1$ rather than $z \sim 2$) compared to the unsmoothed [Madau & Dickinson \(2014\)](#) best-fit function (not shown).

We find that the smoothed [Madau & Dickinson \(2014\)](#) star-formation history is in general agreement with the results obtained through the completely independent approach performed here — with particularly strong agreement at lookback times less than ~ 6 Gyr ($z \sim 0.63$) — lending further evidence that such a fossil record analysis is trustworthy. We suggest that the broader peak obtained here is due to having co-added multiple star-formation histories which have each been smoothed to 0.2 dex rather than simply smoothing a single function by 0.2 dex in the comparison measurement. We argue that this effect could also partly explain the difference in lookback times to the peak in cosmic star formation, although the observed difference is small given the entirely independent approaches of the two methods. Our results also show good quantitative agreement with the cosmic star-formation histories obtained through fossil-record analyses performed by both [López Fernández et al. \(2018\)](#) and [Sánchez et al. \(2019\)](#), and also with the earlier best-fit parametric models to observational redshift studies determined by [Behroozi et al. \(2013\)](#) and [Hopkins & Beacom \(2006\)](#).

If the measured lookback time corresponding to the peak of cosmic star-formation was dictated primarily by artefacts of the SSP templates or of the fitting method, we would expect to find that the peak in each galaxy’s individual star-formation history might be biased towards a certain stellar population age. In such a case, the derived cosmic star-formation history measured in each sample would therefore display its peak at *different* lookback times once galaxies’ observed redshifts are accounted for, since each MaNGA sample targets galaxies from different redshift distributions. The close match between star-formation histories shown in Figure 4 therefore shows that the signal being measured is intrinsic to the data rather than being the product of artefacts. Indeed, we find that the agreement between the star-formation histories measured using each MaNGA sample is *only* seen when the galaxy redshifts are taken into account, and that the above close agreement is smaller than the difference in median lookback times for each sample’s galaxy populations.

We find that increasing the aperture from $1.2 R_e$ to $2.3 R_e$ using the Secondary sample results in a cosmic star-formation history which is greater at all lookback times than [Madau & Dickinson \(2014\)](#)’s best fit to cosmological results. This excess could either be due to overly-conservative aperture corrections or to surface bright-

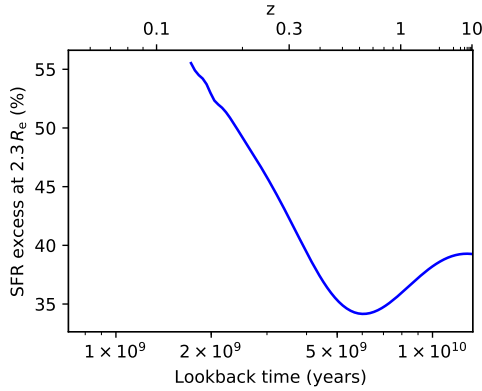


Figure 5. The fractional excess in measured cosmic star formation at all lookback times from the Secondary sample when the aperture is increased from $1.2 R_e$ to $2.3 R_e$. At more recent times, the fractional increase is larger, indicative of inside-out growth occurring in most galaxies.

ness limits causing cosmological studies to have underestimated the total star-formation rates at different redshifts.

Having derived the cosmic star-formation history using the Secondary-sample galaxies with radius limits of $1.2 R_e$ and $2.3 R_e$ separately, we are able to quantify what extra fraction of star-formation is included by increasing the FOV diameter by a factor of ~ 1.9 . Comparison between the two Secondary-derived cosmic star-formation histories of Figure 4 shows that the effect of the increased FOV results in a 35–40% enhancement in the measured star-formation histories at lookback times $\gtrsim 5$ Gyr, increasing to a 55% enhancement by ~ 1.5 Gyr, as illustrated in Figure 5. This increase over time is indicative of inside-out growth resulting in a greater star formation contribution by the galaxy outskirts at more recent times, as we explored for spiral galaxies in Peterken et al. (2020); see also Pérez et al. (2013); Ibarra-Medel et al. (2016); García-Benito et al. (2017); Goddard et al. (2017). It is interesting to note that even at recent times, the ratio in star-formation rate between larger to the smaller aperture of ~ 1.5 is smaller than the corresponding ratio of sky coverage area (~ 3.7), showing that star-formation density is still greatest at galactic centres on average despite the effect of inside-out growth.

5.1 Size²: effects of present-day stellar mass

Having obtained the cosmic star-formation history, we now begin to explore the connection between a galaxy’s present-day physical properties with its historical contribution to the Universe’s star-formation. We split the galaxy sample into five discrete bins of present-day photometrically-measured stellar mass $M_{\star\text{NSA}}$ such that each bin contains an equal (unweighted) number of Primary+ sample galaxies. The thresholds of these bins and the star-formation history of the Universe split into contributions of these mass bins are shown in Figure 6. We have shown the stellar-mass breakdown for the Primary+ sample within $1.2 R_e$, but all other samples’ are similar. We see that the star-formation contribution from higher-mass galaxies becomes less significant at more recent times. For

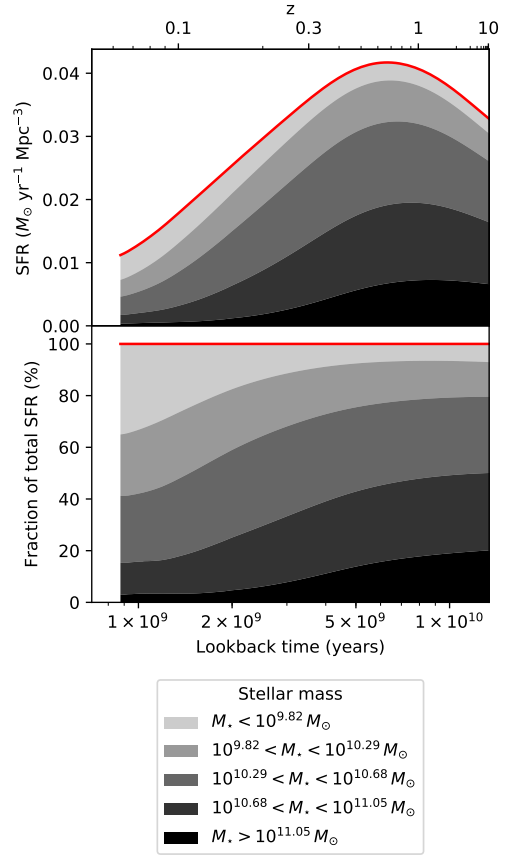


Figure 6. The star-formation history of the Universe stratified by its contributions from galaxies in different present-day stellar mass bins, in absolute star-formation rates (*top*) and by the fractional contribution from each mass bin (*bottom*). Shown is for the Primary+ sample (red line), but all other samples are similar. Higher-mass galaxies have become less dominant in the more recent Universe and vice-versa.

example, galaxies with present-day stellar mass $M_{\star} < 10^{10.29} M_{\odot}$ dominated the cosmic star formation until ~ 2 Gyr ago to contribute only $\sim 50\%$ in the local Universe. We have therefore recovered the known observational effects of downsizing.

A similar perspective of downsizing is gained by measuring the lookback time at which each individual galaxy reached its maximum star-formation rate. The volume-weighted median lookback time t_{peak} of peak star-formation in galaxies as a function of their present-day stellar mass M_{\star} is shown in Figure 7. We find that the peak in star formation typically occurred at $t_{\text{peak}} = 8 \pm 1$ Gyr ago (corresponding to $z \approx 1.1 \pm 0.3$) in the galaxies with the highest present-day stellar masses in the samples ($M_{\star} > 10^{11} M_{\odot}$), falling to $t_{\text{peak}} \lesssim 2$ Gyr ($z \lesssim 0.2$) for galaxies with present-day stellar masses of $M_{\star} < 3 \times 10^9 M_{\odot}$. We also see some signs of downsizing effects being strongest among low-mass galaxies where the gradient $\Delta t_{\text{peak}} / \Delta M_{\star}$ is greatest.

By measuring the lookback time by which galaxies had built the bulk of their present-day stellar mass, Ibarra-Medel et al. (2016), García-Benito et al. (2017), and Peterken et al. (2020) have previously found that low-mass galaxies typically show larger variation in the characteristic formation times than high-mass galaxies. However, we find here that the scatter in t_{peak} remains approximately constant at ~ 0.3 dex over all stellar masses. The two results are not incompatible: we interpret such an apparent dichotomy as indicative

² We are not using “size” here in its usual meaning of a galaxy’s physical or apparent radius or diameter; rather, we mean its stellar mass. Still, such a simple substitution is suitable to sufficiently sustain a satisfactory sibilance with subsequent subheadings.

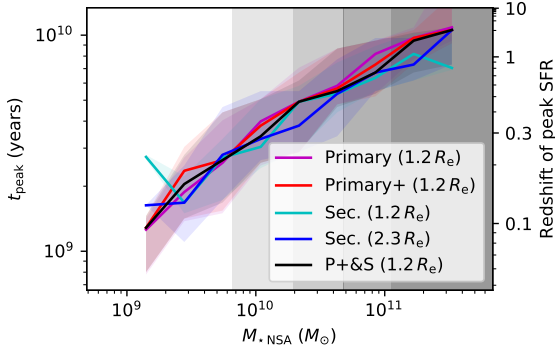


Figure 7. The lookback time to the peak of star-formation t_{peak} as a function of present-day stellar mass $M_{\star,\text{NSA}}$, using each of the MaNGA samples. The solid lines indicate the sample-weighted median values, and the shaded regions lie between the one-third and two-thirds percentiles. Greyscale-shaded background regions indicate the mass bins used in Figure 6 and elsewhere.

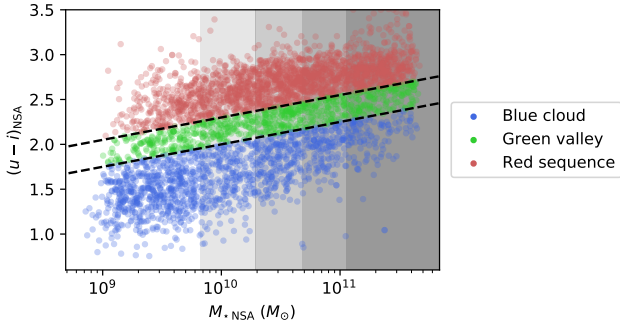


Figure 8. Mass–colour plane of the Primary+ sample galaxies, with galaxies classified according to their colour as used in Section 5.2. Galaxy stellar masses $M_{\star,\text{NSA}}$ and $(u-i)_{\text{NSA}}$ broadband colours are NSA measurements. Shaded backgrounds indicate the bins in stellar mass in Figure 6 and elsewhere.

of low-mass galaxies having greater variation in the rate of decline in star-formation after their common peak time.

Figure 7 again shows strong agreement between each MaNGA sample. We therefore present hereafter only results measured using the Primary+ sample, but results for other samples are similar throughout.

5.2 Shade: effects of present-day colour

By splitting each galaxy sample by the galaxies’ locations on the stellar mass–colour plot, we are also able to investigate the effect of present-day colour on a galaxy’s contribution to the cosmic star-formation history.

5.2.1 Colour classifications

We separate galaxies by their colours according to the following criteria:

- Red sequence: $(u-i)_{\text{NSA}} > 0.25 \log(M_{\star,\text{NSA}}) - 0.2$
- Green valley:

$$0.25 \log(M_{\star,\text{NSA}}) - 0.5 \leq (u-i)_{\text{NSA}} \leq 0.25 \log(M_{\star,\text{NSA}}) - 0.2$$

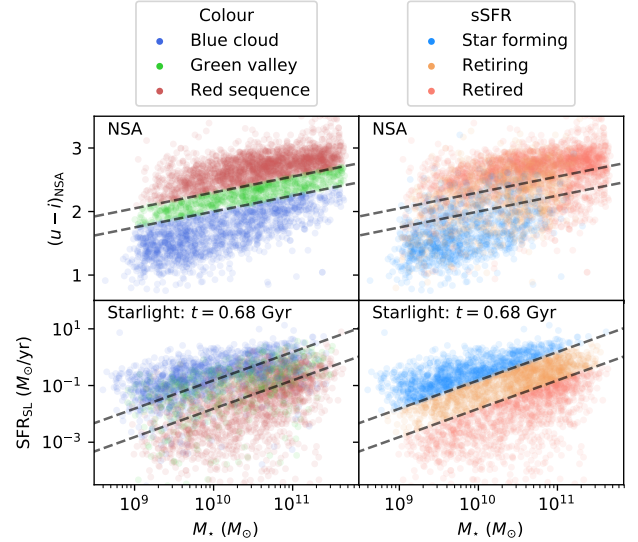


Figure 9. Comparison of galaxies with colour classifications defined in Section 5.2 (left panels, based on $(u-i)_{\text{NSA}}$ broadband colours) and the specific star-formation rate classifications defined in Peterken et al. (2021) (right panels) in the $(u-i)_{\text{NSA}}-M_{\star,\text{NSA}}$ plane (top panels) and $\text{SFR}_{\text{SL}}-M_{\star,\text{SL}}$ plane at a lookback time of $t = 0.68$ Gyr for Primary+ galaxies. The classifications of blue cloud, green valley, and red sequence are analogous to classifications of star-forming, retiring, and retired galaxies respectively. Dashed lines in the top panels indicate the boundaries used to separate blue cloud, green valley, and red sequence galaxies, and those in the bottom panels indicate those used to separate star-forming, retiring, and retired galaxies.

- Blue cloud: $(u-i)_{\text{NSA}} < 0.25 \log(M_{\star,\text{NSA}}) - 0.5$

where the galaxies’ stellar masses $M_{\star,\text{NSA}}$ (measured in M_{\odot}) and $(u-i)_{\text{NSA}}$ broadband colours are taken from the NSA (Blanton et al. 2011) photometry-derived measurements.³ These thresholds and the subsequent classifications of Primary+ galaxies are illustrated in Figure 8.

We showed in Section 4.1 and Equation 2 that broadband colour and specific star-formation rate are closely correlated. To demonstrate how the above colour classifications are linked to star-formation properties, we have also split the galaxy sample into star-forming, retiring, and retired populations using thresholds of $\text{sSFR}_{\text{SL}(t=0.68 \text{ Gyr})} = 10^{-11}$ and 10^{-12} yr^{-1} — as used in Peterken et al. (2021) — where $\text{sSFR}_{\text{SL}(t=0.68 \text{ Gyr})}$ is the ratio of the average STARLIGHT-measured instantaneous star-formation rate to the STARLIGHT-measured instantaneous stellar mass $M_{\star,\text{SL}}$ at a lookback time of $t = 0.68$ Gyr, which is the lowest lookback time measurable with the Primary+ sample as defined in Figure 3. Figure 9 shows a direct comparison of galaxies’ classifications under both schemes on the $(u-i)_{\text{NSA}}-M_{\star,\text{NSA}}$ plane (using NSA-measured colours $(u-i)_{\text{NSA}}$ and stellar masses $M_{\star,\text{NSA}}$) and on the $\text{SFR}_{\text{SL}}-M_{\star,\text{SL}}$ plane at a lookback time of $t = 0.68$ Gyr (using STARLIGHT-derived star-formation rates SFR_{SL} and stellar masses $M_{\star,\text{SL}}$). We find that most star-forming galaxies map onto the blue cloud region,

³ Note that a galaxy’s broadband colour is affected by its inclination due to increased internal dust extinction. We do *not* attempt to correct for this effect, so that our measurements resemble those of other studies of galaxy populations as closely as possible.

most retiring galaxies to the green valley region, and most retired galaxies to the red sequence region, and vice-versa, showing that the $u - i$ colour classifications defined above are broadly analogous to classifications of star formation⁴, and therefore linking the observed measurements to physical galaxy properties.

Having demonstrated the commutativity of broadband colour and specific star-formation rate, it would be feasible to investigate how either of these properties relates to a galaxy’s history. [Ibarra-Medel et al. \(2016\)](#) showed that colour and specific star-formation rate have similar effects on the star-formation history of galaxies. However, since colour is a more readily-measurable property of a galaxy, we will continue to investigate the role of present-day broadband colour rather than present-day specific star-formation rate in the analysis shown here, for more straightforward application of the results to other studies of galaxy populations.

5.2.2 Present-day colour and the star-formation history of the Universe

Figure 10 shows the Primary+-derived star-formation history of the Universe showing the relative contributions from galaxies classified as currently belonging to the blue cloud, the green valley, and the red sequence as defined above. There is a strong correlation between a galaxy’s present-day colour and its past contribution to the total star formation, with the blue cloud contributing only 20% at early times and rising to more than 70% at the present day. We recover how galaxies which are currently exhibiting very low levels of star formation were once the dominant source of new stars.

However, stellar mass and colour classification are not independent galaxy properties, as can be seen in Figure 8. Specifically, high-mass galaxies are more likely to belong to the red sequence and vice-versa. To determine how the effect of present-day colour varies with a galaxy’s stellar mass, we show the relative contribution of each colour classification to each mass bin’s star-formation history in Figure 11. We find that the blue cloud’s increase in contribution to the star-formation history between lookback times of 10 and 1 Gyr varies from a $\sim 20\%$ increase in the highest-mass bin to a $\sim 40\%$ increase in the lowest-mass bins:⁵ a galaxy’s colour is therefore more strongly correlated to its historical contribution to the star-formation history in low-mass than in high-mass galaxies.

We additionally see some evidence for the colour designations reflecting shorter star-formation timescales in low-mass galaxies than in their high-mass counterparts. The most massive blue cloud galaxies began increasing their contribution to that mass bin’s star-formation history ~ 6 Gyr ago to reach its current level ~ 2 Gyr ago, while the lowest-mass bin’s blue cloud only started to become more dominant ~ 2 Gyr ago and appears to still be increasing to the present-day.

We find that galaxies currently in the green valley have contributed an approximately constant 20% to the star-formation history in all mass bins. Such a consistency of the green valley’s contribution between mass bins is to be expected assuming that the timescale

⁴ This strong link is by construction; we chose the $u - i$ broadband colour in Section 4.1 as a proxy for specific star-formation rate due to the sensitivity of u to recent star-formation and i to the total stellar mass. Classifications based on broadband colours at longer wavelengths (e.g. $i - z$) will not be so closely linked to the classifications of specific star-formation rates.

⁵ The discrepancy between these mass-bin values and the increase of $\sim 50\%$ in the blue cloud’s contribution overall is due to the dependent nature of colour and stellar mass: lower-mass bins with a larger fraction of blue cloud galaxies becoming more dominant at more recent times.

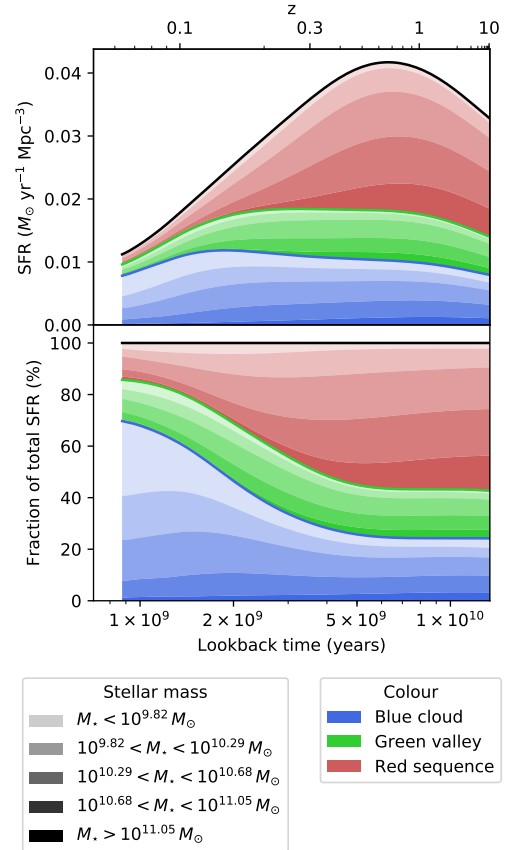


Figure 10. The star-formation history of the Universe inferred from the Primary+ sample, separated into its contributions from galaxies belonging to each galaxy classification (indicated by colours) defined in Section 5.2.1. Each colour classification is also stratified by present-day stellar mass (darkest to lightest shades for most to least massive galaxies) within each broadband colour classification, using the mass bins of Section 5.1. The upper panel shows the total contribution to the star-formation history, while the lower panel shows the fractional contributions to the total star-formation history.

of star-formation transition is independent of stellar mass. However, the constancy of the present-day green valley’s contribution over the last 10 Gyr indicates a complex picture. If these galaxies are those caught in the act of a rapid “quenching” transition from the blue cloud to the red sequence or a rapid rejuvenation transition in the opposite direction, it would be expected that their historical contributions to the cosmic star-formation history should be similar to either the blue cloud’s or the red sequence’s until recent times. The fact that this does not hold true could hint towards the possibility that the galaxies designated as belonging to the green valley using the colour criteria above contain a mix of quenching and rejuvenating galaxies. However, further analysis of the individual star-formation histories of galaxies currently in the green valley shows that this is not true in that most show declining levels of star-formation over the last Gyr, and there is no significant population of rejuvenating green valley galaxies. Instead, it seems that most present-day green valley galaxies have always had low but sustained levels of star-formation, with star-formation histories which have generally followed the star-formation history of the Universe as a whole.

While we do not speculate here as to a possible physical explanation for this observation, it might reflect the slower retiring

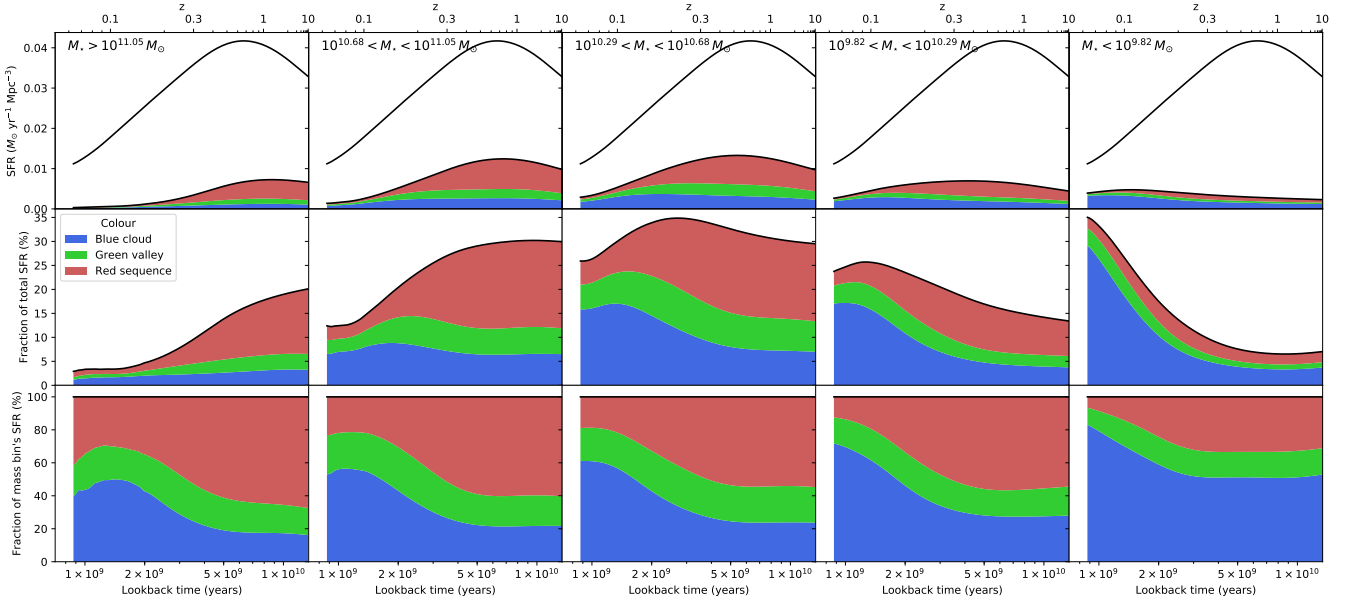


Figure 11. The absolute (*top row*) and fractional (*middle row*) contributions to the star-formation history of the Universe of galaxies of different present-day colour classifications (*colours*) in each mass bin (*columns*; transparencies equivalent to those used in Figure 10), and the relative contribution of each colour classification to each mass bin’s star-formation history (*bottom row*).

processes proposed by Schawinski et al. (2014), for example. Possible drivers of such a “slow quenching” scenario are thought to be predominantly internal processes (Martig et al. 2009; Fang et al. 2013; Bluck et al. 2014; Smethurst et al. 2018; Das et al. 2021). There is observational evidence to suggest that cessation of star-formation occurs on long (several Gyr) timescales in a significant number of galaxies, including ellipticals (see e.g. Smethurst et al. 2015, 2017; Belfiore et al. 2018; Lacerna et al. 2020), although other studies argue otherwise (see e.g. Bremer et al. 2018).

By considering how galaxies of each colour classification in the five bins of stellar mass used in Section 5.1 have contributed to the cosmic star-formation history, we see in Figure 10 some signs of downsizing effects being present in all colour classifications; low-mass galaxies of all colours become relatively more dominant at smaller lookback times. To measure how downsizing effects vary between colour classifications in this way, we also show the relative contribution of galaxies in each mass bin to each colour classification’s star-formation history in Figure 12. We find evidence for downsizing having occurred most strongly in galaxies currently in the blue cloud, with galaxies in the two lowest-mass bins increasing their contribution by 20% in the red sequence and 30% in the blue cloud, with the green valley lying in between.

This difference in the strength of the downsizing effect seen in galaxies of different colour classifications is illustrated further in Figure 13, where we see that red sequence galaxies reached peak star formation at earlier times than green valley or blue cloud galaxies at all stellar masses, but that this effect is greatest in low-mass galaxies.

5.3 Shape: effects of present-day morphology

Having quantitatively measured the link between a galaxy’s present day colour and its historical contribution to the cosmic star-formation history, we can now independently assess the relative role of a galaxy’s present-day morphology.

5.3.1 Morphological classifications

Over 91% of galaxies in all MaNGA samples have been classified by the Galaxy Zoo “citizen science” project (Lintott et al. 2008), in which volunteers are asked to classify galaxies’ morphological features. We make use of the redshift-debiased vote fractions of Hart et al. (2016) from Galaxy Zoo 2 (Willett et al. 2013) to split the galaxy samples by their present-day morphology. We classify each galaxy according to the following criteria:

- Elliptical: $p_{\text{features or disk}} < 0.5$
- S0: $p_{\text{features or disk}} > 0.5$ and $p_{\text{spiral}} < 0.5$
- Spiral: $p_{\text{features or disk}} > 0.5$ and $p_{\text{spiral}} > 0.5$

where $p_{[\text{class}]} > 0.5$ indicates the debiased vote fraction for [class] from Hart et al. (2016). These thresholds were chosen to minimise the number of unclassifiable or ambiguous galaxies, and are therefore less stringent than those recommended by Willett et al. (2013), and hence open to significant contamination between morphological classes.

The stellar mass–colour distribution of the Primary+ galaxies indicating their Galaxy Zoo morphologies is shown in the upper panel of Figure 14. Over most of the sample’s range in stellar mass, the spirals occupy the bluer region of parameter space, but at the low-mass ($< 2 \times 10^9 M_{\odot}$) end, blue galaxies are likely to have been classified as earlier-type galaxies, as we noted in Peterken et al. (2021). This unexpected trend is likely because spiral structure in low-mass disk galaxies is harder to discern in SDSS imagery due to resolution effects. The classifications we have implemented from the vote fractions to minimise the number of unclassified galaxies will therefore result in a high level of contamination between morphologies. A lower spiral vote-fraction threshold might more reliably distinguish between morphologies in low-mass galaxies, but only at the expense of increasing the number of high-mass early-type disk galaxies being mis-classified as spirals. Alternatively, using the recommended criteria of Willett et al. (2013) to obtain clean samples

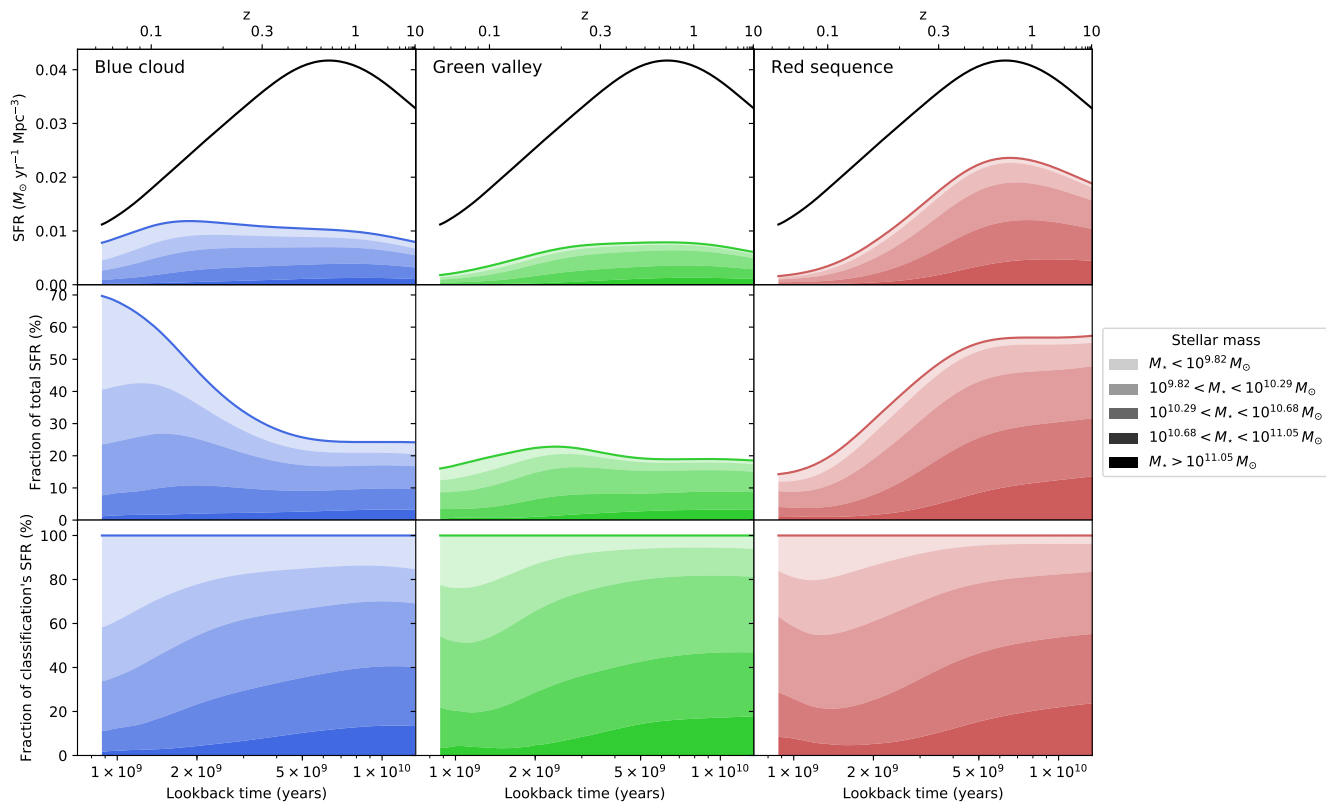


Figure 12. The absolute (*top row*) and fractional (*middle row*) contributions to the star-formation history of the Universe of galaxies of different stellar masses in each colour classification, and the relative contribution of galaxies with different stellar mass to each colour classification’s star-formation history (*bottom row*).

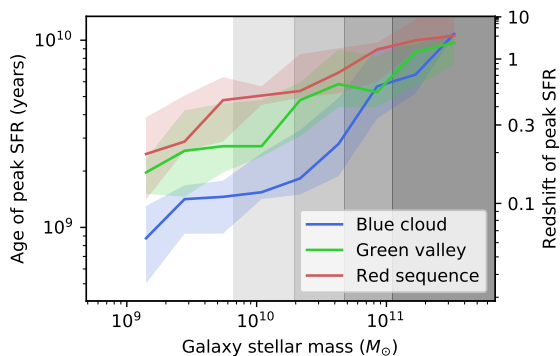


Figure 13. The lookback time to the peak star formation rate of galaxies currently belonging to each of the colour classifications. Solid lines indicate median values, and shaded regions lie between the one- and two-third percentiles. Blue cloud galaxies peaked in star formation more recently and show stronger downsizing effects than red sequence galaxies.

of galaxies of each morphology creates a large number of unclassified “ambiguous” galaxies, which when removed from the sample will render the MaNGA sample weightings described in Section 3.1 inaccurate. However, we have repeated the analysis using debiased vote fraction thresholds of 80% instead of 50% in the criteria above and found no change to the results at high stellar masses, but at low stellar masses the dominance of galaxies with “ambiguous” morphologies makes any quantitative results impossible.

Alternative morphological classifications using the deep learn-

ing methods developed by Domínguez Sánchez et al. (2018) are available for galaxies which were part of the SDSS data release 15 (DR15; Aguado et al. 2019). This approach uses Galaxy Zoo and Nair & Abraham (2010) classifications as training sets to classify SDSS galaxy images. Instead of replicating vote fractions for the presence of morphological features in each galaxy, the Domínguez Sánchez et al. (2018) approach directly provides a prediction for each galaxy’s morphological T-type. The resulting separation of different morphologies is cleaner at low stellar masses in the colour–mass plane, as illustrated in the lower panel of Figure 14. The question then arises of which classification method should be used. Fortunately, in most cases we find that the results presented here do not change depending on which classification we use and we have therefore primarily presented results using the Galaxy Zoo classifications to make use of the larger sample size. In the instances where we find that the two classification methods provide conflicting results, we will describe and discuss those differences.

5.3.2 Present-day morphology and the star-formation history of the Universe

The cosmic star-formation history separated into contributions from galaxies of different present-day stellar masses and the Galaxy Zoo morphologies is shown in Figure 15. Present-day spiral galaxies have contributed the greatest amount (at least 40%) to the total star formation of any morphology at all lookback times, and contribute the majority (60%) at the present day. This 20% morphology effect on a galaxy’s past contribution to the star-formation history of the

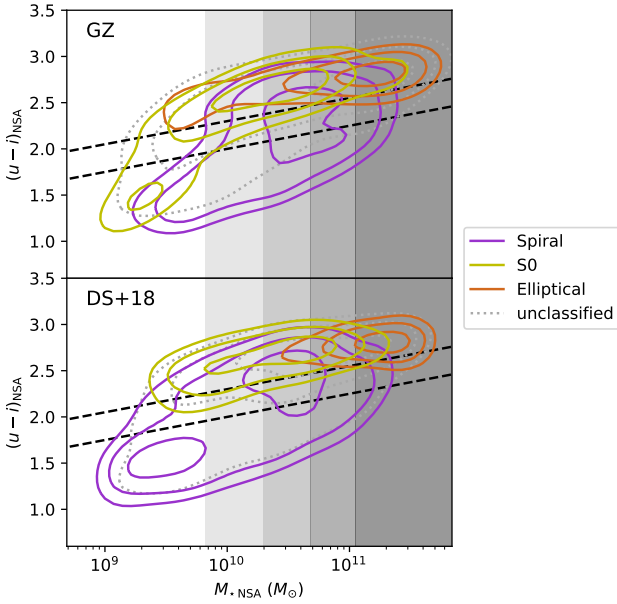


Figure 14. The distribution of galaxies in the stellar mass–colour plane (as Figure 8), with galaxies coloured by their Galaxy Zoo (*top*) and Domínguez Sánchez et al. (2018) machine learning (*bottom*) morphological classifications as used in Section 5.3. Spiral galaxies occupy the blue region of this parameter space in both schemes. There is ambiguity at low stellar masses where the Galaxy Zoo classifications are less reliable due to difficulties in distinguishing spiral structure in SDSS imagery and the low thresholds used for separating morphologies. Galaxies with low stellar mass are more likely to have spiral-morphology machine learning classifications compared to their Galaxy Zoo classifications. Contours of 30%, 50%, and 80% of the peak unweighted density are shown for each classification. For reference, dashed black lines delineate the boundaries between the colour classifications used in Section 5.2, and shaded background regions indicate the stellar mass bins used throughout.

Universe is smaller than the 40% colour increase seen in Figure 10, implying that colour is a stronger indicator of a galaxy’s full star-formation history than morphology, as found by others (e.g. Ibarra-Medel et al. 2016).

We find that a galaxy’s morphology only reflects the last 2 – 3 Gyr of its star-formation history on average, in that the relative contributions to the cosmic star-formation history by galaxies of different morphologies did not change until this lookback time. We have previously demonstrated this result in more detail (see Peterken et al. 2021).

However, morphology and mass are correlated, as shown in Figure 14: observed morphology effects could be simply a result of early-type galaxies having higher stellar mass on average, and will therefore exhibit star-formation histories with higher star-formation rates at earlier lookback times than their late-type and less massive counterparts, as we saw in Figure 7. To properly distinguish between downsizing and morphological effects, Figure 16 shows the same data as in Figure 15 but with each mass bin separated. We find that regardless of the morphological composition of the mass bin, spirals have increased their contribution to the star-formation history by $\sim 20\%$ between lookback times of 10 and 1 Gyr. We therefore find the effects of present-day morphology on the contribution to the star-formation history of the Universe to be independent of present-day stellar mass.

However, we also see some evidence for the morphological

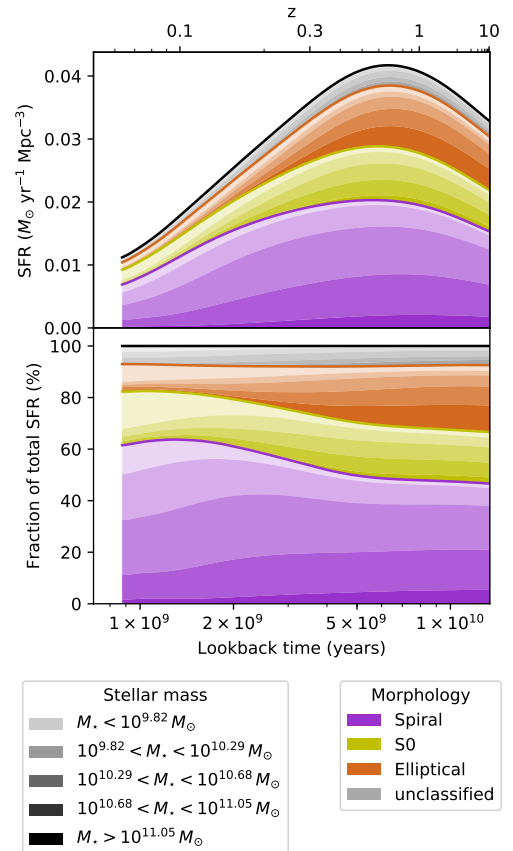


Figure 15. The star-formation history of the Universe inferred from the Primary+ sample, stratified into its contributions from galaxies in different stellar mass bins (shades; darkest to lightest for most- to least-massive galaxies) and of different Galaxy Zoo morphologies (colours), analogous to Figure 10. The *top* panel shows the star-formation history, and the *bottom* panel shows the percentage contribution from each of the sample’s subdivisions to the total cosmic star-formation history. Machine learning morphologies of Domínguez Sánchez et al. (2018) show similar results.

classifications reflecting different timescales of star-formation histories in different mass bins in the same manner as we saw for the colour classifications in Figure 11. Spiral galaxies with the largest present-day stellar mass began increasing in their contribution to their mass bin’s star-formation history ~ 4 Gyr ago to reach the current level ~ 2 Gyr ago, compared to ~ 2 Gyr ago for the lowest-mass spirals to start increasing their contribution with a trend of continued increase.

As in Figure 10, we are also able to reorganise the area plot of Figure 15 by morphology, to show how galaxies of different present-day stellar masses have contributed to each morphological classification’s star-formation history to reveal how the effects of stellar mass change among galaxies of different morphologies, as shown in Figure 17. For the Galaxy Zoo morphologies, we find that downsizing effects are stronger in earlier-type galaxies; galaxies in the lowest-mass bin become more dominant among lenticular and elliptical galaxies at smaller lookback times than the equivalent effect in spiral galaxies.

However, when using the Domínguez Sánchez et al. (2018) machine learning morphological classifications — as shown in Figure 18 — we find the opposite; spiral galaxies show stronger downsizing effects than lenticular or elliptical galaxies. We also find that

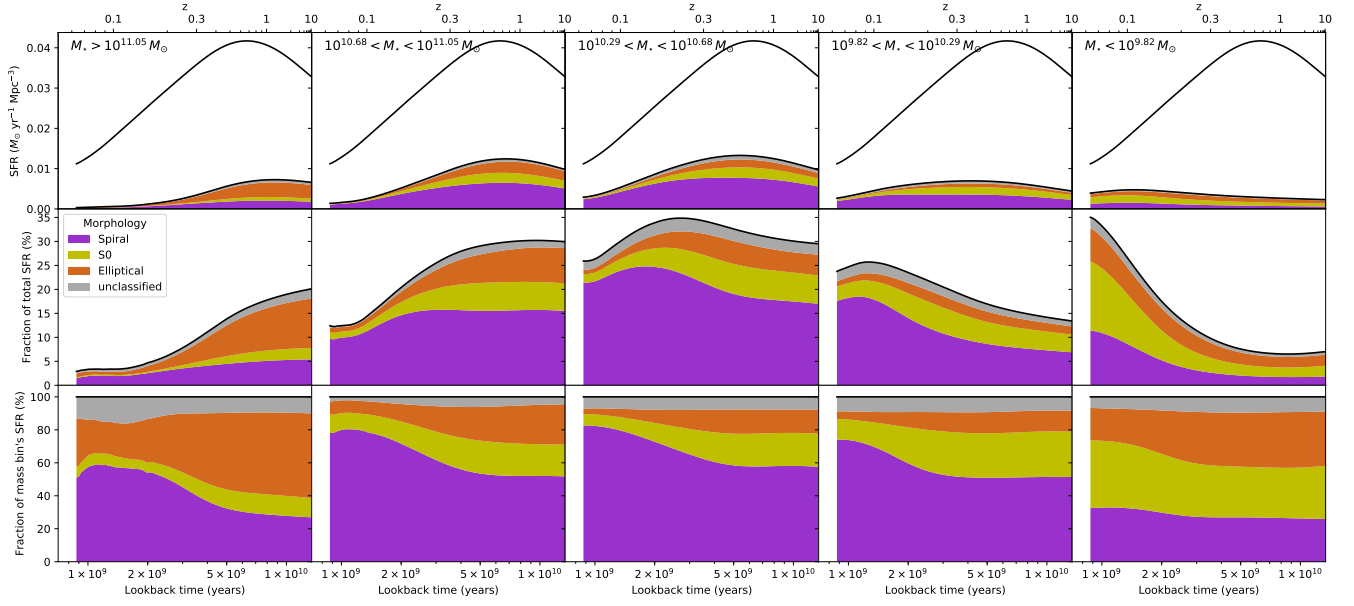


Figure 16. The absolute (*top row*) and fractional (*middle row*) contributions to the star-formation history of the Universe of galaxies of different morphologies in each bin of stellar mass (*columns*), and the relative contribution of different Galaxy Zoo morphologies to each mass bin's star-formation history (*bottom row*). Analogous to Figure 11.

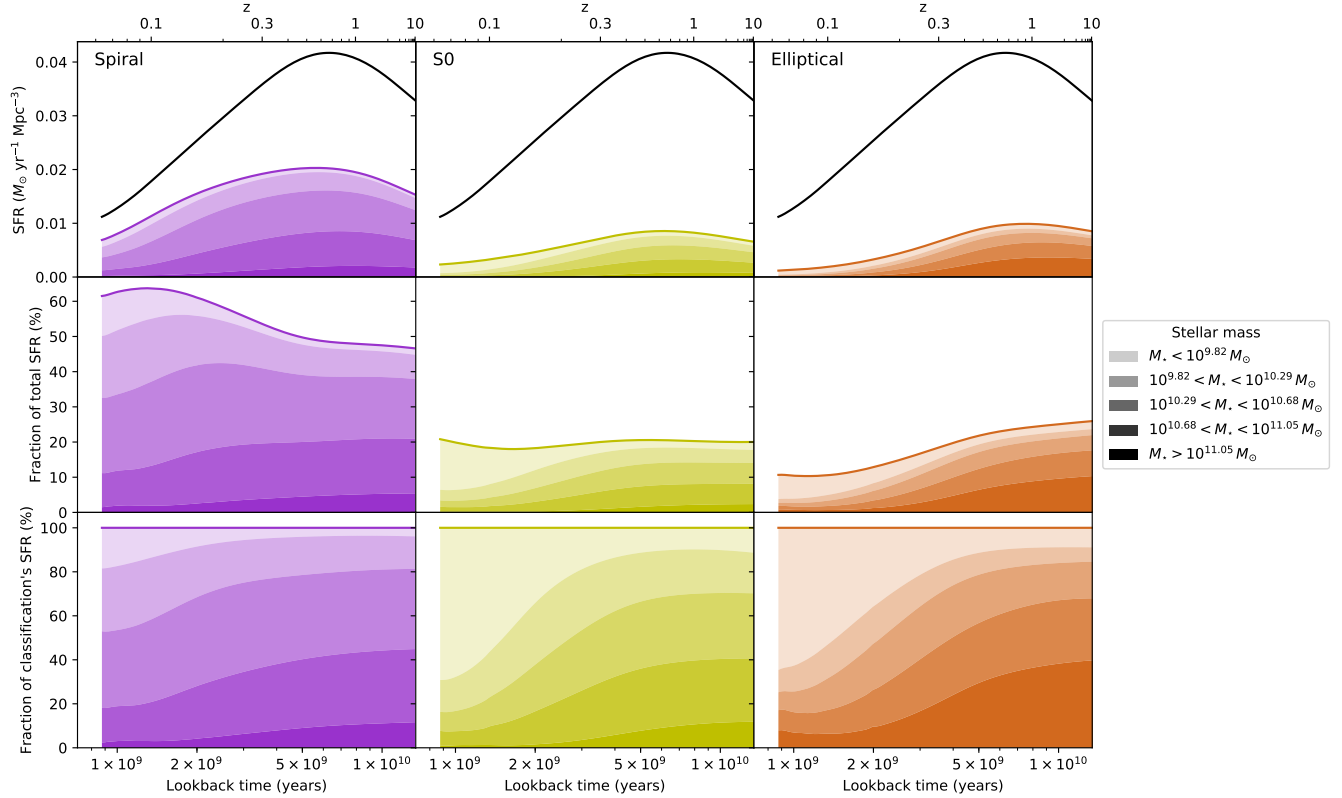


Figure 17. The absolute (*top row*) and fractional (*middle row*) contributions to the star-formation history of the Universe of galaxies with different present-day Galaxy Zoo morphologies, stratified by the contributions from each stellar mass bin. The relative contribution of galaxies with different stellar mass to each morphology's star-formation history is also shown (*bottom row*). Analogous to Figure 12.

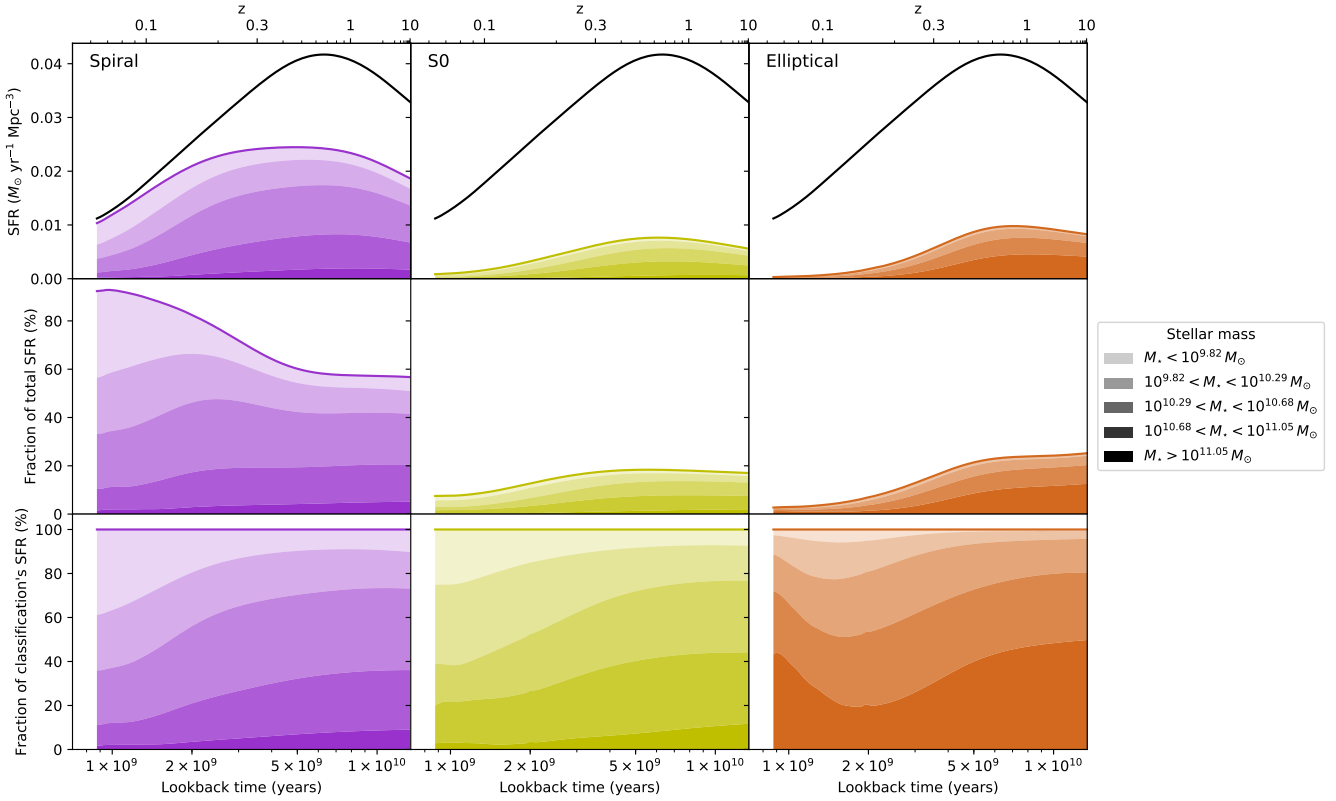


Figure 18. As Figure 17 but using the Domínguez Sánchez et al. (2018) machine learning morphologies. The galaxies which were not included in DR15 have been removed, and the weights of the remaining galaxies have been scaled such that the total weighted mass in the sample remains the same. The total star-formation history for the *full* Primary+ sample (black line) is shown, resulting in the sum of all shown contributions from each morphology to not equal exactly 100% of the total at some lookback times.

elliptical galaxies have contributed almost no star formation in the last ~ 2 Gyr. This difference highlights how carefully morphological classifications must be used to avoid biases associated with the difficulties inherent in identifying structures in low-mass galaxies.

The observed differences are easily explained by uncertainty in the classification of low-mass spiral galaxies, which appears to be more reliably resolved by the machine learning approach. We wish to stress here that such a discrepancy merely highlights the importance of careful consideration of what exact morphological classifications are being used, and *does not* imply that Galaxy Zoo classifications are inherently flawed. Instead, we argue that studies using any morphological classification method should be wary of how galaxies with potentially ambiguous morphologies are treated. This is especially important if the classification scheme is based on a “pure” Hubble approach, which often contains significant subjectivity (Naim et al. 1995) and assumptions (Freeman 1970; Hart et al. 2017, 2018; Masters et al. 2019), and does not necessarily reflect the physical processes occurring within galaxies (Cappellari 2016; Wang et al. 2020). Indeed, we note again here that the implementation of morphological classifications using Galaxy Zoo vote fractions described in Section 5.3.1 goes contrary to the advice of Willett et al. (2013), who detail how low-contamination samples of Galaxy Zoo galaxies with any required morphology can be effectively obtained.

In Figure 18 (and to a lesser extent also in Figure 17), we see some apparent “upsizing” occurring in elliptical galaxies; high-mass galaxies appear to increase their relative contribution to the

star-formation history of all ellipticals in the last ~ 2 Gyr. This phenomenon is likely due to the problems that we addressed in Peterken et al. (2020) of the “UV upturn” (see also Yi 2008; Cid Fernandes & González Delgado 2010) being most dominant in high-mass ellipticals due to their extremely old stellar populations. That this effect is strongest using the Domínguez Sánchez et al. (2018) morphological classifications is therefore due to the population of possibly misclassified low-mass galaxies in the Galaxy Zoo classifications diluting the effect with “real” star formation; see also Fischer et al. (2019, Section 4.4) who describe this phenomenon in more detail. However, we note that the observed effects are extremely small; even with this spurious increase of star-formation rate in high-mass elliptical galaxies, those galaxies still only account for $< 1\%$ of the star formation in the present-day Universe regardless of which morphological classification method is used, so these effects do not significantly affect the derived cosmic star-formation history.

We find the total star-formation histories of all galaxies with stellar mass $M_{\star} > 10^{10.29} M_{\odot}$ (i.e. in the three bins of greatest stellar mass) to be similar for lenticular and elliptical classifications. This similarity could imply that all massive present-day early-type galaxies have experienced similar star-formation histories, with the difference in morphologies due to other factors such as merger rate histories. Alternatively, it could be evidence for visually-determined shape being an ineffective way to separate the bimodality of fast- and slow-rotating early-type galaxies (Emsellem et al. 2007; Cappellari et al. 2011; Cappellari 2016; Graham et al. 2018), or a combination of both of these effects.

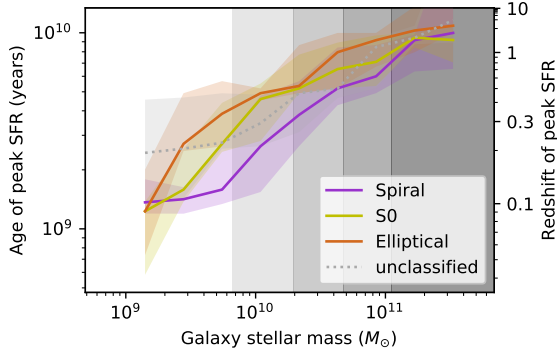


Figure 19. The peak in star-formation history of galaxies of each present-day morphological classification in the Primary+ sample, as determined using Galaxy Zoo. Solid lines indicate the weighted medians and the coloured shaded regions enclose the area between the one- and two-thirds weighted percentiles.

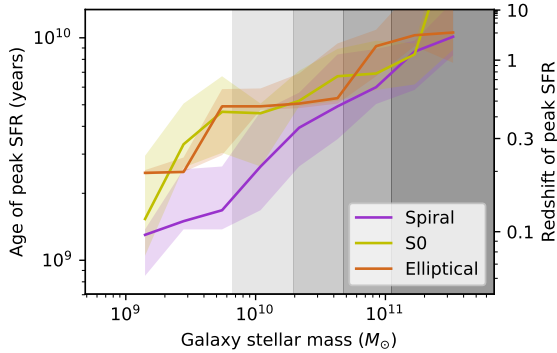


Figure 20. As Figure 19, but using the Domínguez Sánchez et al. (2018) machine learning morphological classifications of DR15 galaxies.

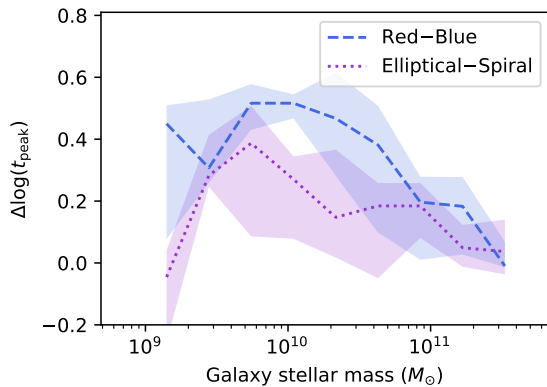


Figure 21. The offset $\Delta \log(t_{\text{peak}})$ in lookback time of peak star-formation rate t_{peak} observed between present-day red sequence and blue cloud galaxies (blue dashed line), and between present-day elliptical and spiral galaxies (purple dotted line) using Galaxy Zoo classifications, as a function of present-day galaxy stellar mass M_{\star} . The effect of present-day colour is larger than that of present-day morphology at all stellar masses, but is particularly significant in the range $7 \times 10^9 M_{\odot} \lesssim M_{\star} \lesssim 4 \times 10^{10} M_{\odot}$.

By comparing the lookback time of peak star formation of galaxies with different present-day morphologies in Figures 19 (for Galaxy Zoo morphologies) and 20 (for Domínguez Sánchez et al. (2018) machine learning morphologies), we see that spiral galaxies peaked more recently than early-type galaxies at all present-day stellar masses regardless of the classification method. We find that this difference is greater in galaxies with low stellar mass, and is greatest around $M_{\star} = 6 \times 10^9 M_{\odot}$; above this threshold we find that both classification schemes display stronger downsizing among spirals than in early-type galaxies, in agreement with Goddard et al. (2017).

We also find that the peak in star-formation history of lenticular and elliptical galaxies is similar for early-type galaxies with stellar masses $M_{\star} > \sim 10^{10} M_{\odot}$ using the Galaxy Zoo classifications (Figure 19) and for stellar masses $M_{\star} > \sim 10^9 M_{\odot}$ using the Domínguez Sánchez et al. (2018) classifications (Figure 20), again reflecting either the similar histories of these galaxies or the difficulty in distinguishing between them through imagery alone. We see that the star-formation peak in present-day lenticular galaxies classified by Galaxy Zoo becomes systematically more recent for lower stellar masses, highlighting likely contamination of mis-classified spiral galaxies using the thresholds applied here.

However, regardless of which classification method is used, we see again that the effect of morphology on a galaxy’s contribution to the cosmic star-formation history is smaller than the effect of colour: the difference in peak star-formation times between early- and late-type galaxies is smaller than the difference between blue cloud and red sequence galaxies (~ 0.2 dex and ~ 0.5 dex respectively at $M_{\star} = 10^{10} M_{\odot}$ for example). This is illustrated at all present-day stellar masses in Figure 21.

6 SIZE VERSUS SHADE VERSUS SHAPE: CONCLUSIONS AND INTERPRETATION

Here, we have recovered evidence for downsizing, in that the fraction of star-formation occurring in the galaxies with greatest present-day stellar mass was largest at early times, with low-mass galaxies dominating the cosmic star-formation at more recent times, and that the lookback time corresponding to a galaxy’s peak star-formation rate is therefore correlated with its present-day stellar mass. We find that this correlation exhibits the strongest gradient among low-mass galaxies, suggesting accelerating downsizing at more recent times. By further splitting the galaxy sample, we subsequently showed that downsizing effects are present in galaxies of all present-day colours (which we showed to be analogous to specific star-formation rate) and morphologies. A galaxy’s present-day stellar mass is therefore a significant indicator of its star-formation history regardless of its other properties.

In quantifying these effects, we found that galaxies currently in the blue cloud exhibited stronger downsizing effects than those in the green valley or red sequence. However, we found some differences in whether downsizing is strongest in present-day early- or late-type galaxies depending on which classification method was used, which we argue is due to our non-standard implementation of Galaxy Zoo morphologies, and therefore highlights the care that must be taken when separating galaxies by their visual morphologies. Reassuringly, there is agreement that late-type galaxies exhibit the stronger downsizing effects among galaxies with stellar mass $M_{\star} > 6 \times 10^9 M_{\odot}$ and that high-mass elliptical and lenticular galaxies have had similar star-formation histories.

Irrespective of classification scheme, we find that the effect

of present-day colour is greater than the effect of present-day morphology on a galaxy’s star-formation history — confirming previous results (Ibarra-Medel et al. 2016; García-Benito et al. 2019) — in that the contribution from present-day blue cloud galaxies increased by $\sim 40\%$ over the past 10 Gyr but that from spirals only increased by $\sim 20\%$ over the same time period by comparison. Similarly, although we found that present-day spirals and blue cloud galaxies exhibited the more recent peaks in star-formation at all stellar masses, the typical difference between spiral and elliptical galaxies (~ 0.3 dex) is less than that between blue cloud and red sequence galaxies (~ 0.6 dex). These results suggest that galaxies of similar morphologies are more likely to have undergone more significantly different histories compared to the equivalent variation in histories among galaxies of similar colours.

However, we also find evidence that these straightforward results do not tell the complete story. Specifically, we find that both present-day colour and morphology reflect only the more recent star-formation histories among lower-mass galaxies compared to their counterparts with high stellar mass. We interpret this as reflective of a galaxy’s inertia to change. The physical processes required to suppress or rejuvenate star-formation or to restructure a galaxy must occur over longer timescales to significantly alter a massive galaxy’s observed properties. Meanwhile, the tidal, stripping, starvation, or inflow processes experienced by less massive galaxies are able to affect their star-formation rates (and therefore colours) and morphologies much more rapidly.

We have therefore demonstrated that a galaxy’s mass, colour and morphology — size, shade and shape — all indicate its historical contribution to the cosmic star-formation history, but to different extents and with codependencies such that all three properties must be considered to build a full picture.

7 SUMMARY

Using an established stellar population “fossil record” analysis, we obtained star-formation histories of the inner $1.2 R_e$ of 6861 galaxies from the SDSS-IV MaNGA survey, with 2519 galaxies also sampled to $2.3 R_e$. By carefully weighting each galaxy to create an effectively volume-limited sample, we inferred the star-formation history of the Universe, which was found to be in general agreement with previous observations of galaxy populations at different redshifts.

We showed that a galaxy’s star-formation history is linked to its present-day mass, its colour, and its morphology, although colour is more strongly connected than morphology regarding historical contributions to the cosmic star-formation history. We also found evidence for downsizing effects being significant in galaxies of all present-day colours and morphologies, in that low-mass galaxies of all types have become more dominant in their contribution to the cosmic star-formation rate in more recent times. These effects, however, were found to be most significant among galaxies currently in the blue cloud. Different morphological classification schemes gave contradictory results on whether downsizing is strongest among galaxies designated as being currently early or late type, but show agreement that spiral galaxies exhibit the stronger effects among galaxies with present-day stellar mass $M_\star > 6 \times 10^9 M_\odot$.

We also found that the historical contribution to the cosmic star-formation history from galaxies currently in the “green valley” does not directly follow that of either the blue cloud or the red sequence populations, with these galaxies’ star-formation histories being remarkably representative of that of the Universe as a whole.

These results once again demonstrate the power of stellar pop-

ulation fossil record techniques in uncovering the link between the Universe’s past with the galaxies we see today.

8 DATA AVAILABILITY

This publication uses the team-internal MPL-9 version of the MaNGA science data products, which are broadly similar to previous versions available publicly through SDSS Data Releases DR13 (Albareti et al. 2017), DR14 (Abolfathi et al. 2018), and DR15 (Aguado et al. 2019). Comparable data products containing the full MaNGA galaxy sample — including the full sample used here — will be publicly released in 2021 as part of SDSS DR17, as will the raw data and all previous versions of the data reduction pipeline.

ACKNOWLEDGEMENTS

The authors thank the anonymous reviewer for their helpful suggestions and improvements to this paper.

The authors also thank S. F. Sánchez, D. Wake, A. R. Calette and A. Rodríguez-Puebla for their extensive help and support on the technical aspects of this work.

Funding for the Sloan Digital Sky Survey IV has been provided by the Alfred P. Sloan Foundation, the U.S. Department of Energy Office of Science, and the Participating Institutions. SDSS acknowledges support and resources from the Center for High-Performance Computing at the University of Utah. The SDSS web site is www.sdss.org.

SDSS is managed by the Astrophysical Research Consortium for the Participating Institutions of the SDSS Collaboration including the Brazilian Participation Group, the Carnegie Institution for Science, Carnegie Mellon University, the Chilean Participation Group, the French Participation Group, Harvard-Smithsonian Center for Astrophysics, Instituto de Astrofísica de Canarias, The Johns Hopkins University, Kavli Institute for the Physics and Mathematics of the Universe (IPMU) / University of Tokyo, the Korean Participation Group, Lawrence Berkeley National Laboratory, Leibniz Institut für Astrophysik Potsdam (AIP), Max-Planck-Institut für Astronomie (MPIA Heidelberg), Max-Planck-Institut für Astrophysik (MPA Garching), Max-Planck-Institut für Extraterrestrische Physik (MPE), National Astronomical Observatories of China, New Mexico State University, New York University, University of Notre Dame, Observatório Nacional / MCTI, The Ohio State University, Pennsylvania State University, Shanghai Astronomical Observatory, United Kingdom Participation Group, Universidad Nacional Autónoma de México, University of Arizona, University of Colorado Boulder, University of Oxford, University of Portsmouth, University of Utah, University of Virginia, University of Washington, University of Wisconsin, Vanderbilt University, and Yale University.

This publication uses data generated via the Zooniverse.org platform, development of which is funded by generous support, including a Global Impact Award from Google, and by a grant from the Alfred P. Sloan Foundation.

We are grateful for access to the University of Nottingham’s Augusta high performance computing facility.

REFERENCES

- Abolfathi B., et al., 2018, *ApJS*, **235**, 42
 Aguado D. S., et al., 2019, *ApJS*, **240**, 23

- Albareti F. D., et al., 2017, *ApJS*, **233**, 25
- Asa'd R. S., Vazdekis A., Cerviño M., Noël N. E. D., Beasley M. A., Kassab M., 2017, *MNRAS*, **471**, 3599
- Behroozi P. S., Wechsler R. H., Conroy C., 2013, *ApJ*, **770**, 57
- Belfiore F., et al., 2018, *MNRAS*, **477**, 3014
- Belfiore F., et al., 2019, *AJ*, **158**, 160
- Bell E. F., et al., 2012, *ApJ*, **753**, 167
- Bellstedt S., et al., 2020, arXiv e-prints, p. arXiv:2005.11917
- Blanton M. R., Moustakas J., 2009, *ARA&A*, **47**, 159
- Blanton M. R., Kazin E., Muna D., Weaver B. A., Price-Whelan A., 2011, *AJ*, **142**, 31
- Blanton M. R., et al., 2017, *AJ*, **154**, 28
- Bluck A. F. L., Mendel J. T., Ellison S. L., Moreno J., Simard L., Patton D. R., Starkenburg E., 2014, *MNRAS*, **441**, 599
- Bremer M. N., et al., 2018, *MNRAS*, **476**, 12
- Bundy K., et al., 2015, *ApJ*, **798**, 7
- Calzetti D., Armus L., Bohlin R. C., Kinney A. L., Koornneef J., Storchi-Bergmann T., 2000, *ApJ*, **533**, 682
- Cappellari M., 2016, *ARA&A*, **54**, 597
- Cappellari M., et al., 2011, *MNRAS*, **416**, 1680
- Catalán-Torrecilla C., et al., 2015, *A&A*, **584**, A87
- Chabrier G., 2003, *PASP*, **115**, 763
- Charlot S., Worthey G., Bressan A., 1996, *ApJ*, **457**, 625
- Cherinka B., et al., 2019, *AJ*, **158**, 74
- Cheung E., et al., 2012, *ApJ*, **760**, 131
- Cid Fernandes R., 2018, *MNRAS*, **480**, 4480
- Cid Fernandes R., González Delgado R. M., 2010, *MNRAS*, **403**, 780
- Cid Fernandes R., Mateus A., Sodré L., Stasińska G., Gomes J. M., 2005, *MNRAS*, **358**, 363
- Cid Fernandes R., et al., 2013, *A&A*, **557**, A86
- Cid Fernandes R., et al., 2014, *A&A*, **561**, A130
- Connolly A. J., Szalay A. S., Dickinson M., SubbaRao M. U., Brunner R. J., 1997, *ApJ*, **486**, L11
- Conroy C., Gunn J. E., 2010, *ApJ*, **712**, 833
- Conroy C., Gunn J. E., White M., 2009, *ApJ*, **699**, 486
- Conroy C., White M., Gunn J. E., 2010, *ApJ*, **708**, 58
- Cowie L. L., Songaila A., Hu E. M., Cohen J. G., 1996, *AJ*, **112**, 839
- Das A., Pandey B., Sarkar S., 2021, arXiv e-prints, p. arXiv:2101.02564
- Domínguez Sánchez H., Huertas-Company M., Bernardi M., Tuccillo D., Fischer J. L., 2018, *MNRAS*, **476**, 3661
- Drory N., et al., 2015, *AJ*, **149**, 77
- Emsellem E., et al., 2007, *MNRAS*, **379**, 401
- Fang J. J., Faber S. M., Koo D. C., Dekel A., 2013, *ApJ*, **776**, 63
- Fischer J. L., Domínguez Sánchez H., Bernardi M., 2019, *MNRAS*, **483**, 2057
- Fontanot F., De Lucia G., Monaco P., Somerville R. S., Santini P., 2009, *MNRAS*, **397**, 1776
- Fraser-McKelvie A., et al., 2019, *MNRAS*, **488**, L6
- Freeman K. C., 1970, *ApJ*, **160**, 811
- García-Benito R., et al., 2017, *A&A*, **608**, A27
- García-Benito R., González Delgado R. M., Pérez E., Cid Fernandes R., Sánchez S. F., de Amorim A. L., 2019, *A&A*, **621**, A120
- Ge J., Yan R., Cappellari M., Mao S., Li H., Lu Y., 2018, *MNRAS*, **478**, 2633
- Ge J., Mao S., Lu Y., Cappellari M., Yan R., 2019, *MNRAS*, **485**, 1675
- Goddard D., et al., 2017, *MNRAS*, **466**, 4731
- González Delgado R. M., et al., 2016, *A&A*, **590**, A44
- González Delgado R. M., et al., 2017, *A&A*, **607**, A128
- Graham M. T., et al., 2018, *MNRAS*, **477**, 4711
- Greener M. J., et al., 2020, *MNRAS*,
- Gunn J. E., et al., 2006, *AJ*, **131**, 2332
- Hart R. E., et al., 2016, *MNRAS*, **461**, 3663
- Hart R. E., et al., 2017, *MNRAS*, **472**, 2263
- Hart R. E., Bamford S. P., Keel W. C., Kruk S. J., Masters K. L., Simmons B. D., Smethurst R. J., 2018, *MNRAS*, **478**, 932
- Heavens A., Panter B., Jimenez R., Dunlop J., 2004, *Nature*, **428**, 625
- Holmberg E., 1958, Meddelanden fran Lunds Astronomiska Observatorium Serie II, **136**, 1
- Hopkins A. M., Beacom J. F., 2006, *ApJ*, **651**, 142
- Ibarra-Medel H. J., et al., 2016, *MNRAS*, **463**, 2799
- Kennicutt R. C. J., 1983, *ApJ*, **272**, 54
- Kennicutt Jr. R. C., 1998, *ARA&A*, **36**, 189
- Lacerna I., Ibarra-Medel H., Avila-Reese V., Hernández-Toledo H. M., Vázquez-Mata J. A., Sánchez S. F., 2020, *A&A*, **644**, A117
- Law D. R., et al., 2015, *AJ*, **150**, 19
- Law D. R., et al., 2016, *AJ*, **152**, 83
- Lee H.-c., Worthey G., Trager S. C., Faber S. M., 2007, *ApJ*, **664**, 215
- Li H., et al., 2017, *ApJ*, **838**, 77
- Lintott C. J., et al., 2008, *MNRAS*, **389**, 1179
- López Fernández R., et al., 2018, *A&A*, **615**, A27
- Madau P., Dickinson M., 2014, *ARA&A*, **52**, A17
- Madau P., Ferguson H. C., Dickinson M. E., Giavalisco M., Steidel C. C., Fruchter A., 1996, *MNRAS*, **283**, 1388
- Maraston C., 1998, *MNRAS*, **300**, 872
- Maraston C., 2005, *MNRAS*, **362**, 799
- Martig M., Bournaud F., Teyssier R., Dekel A., 2009, *ApJ*, **707**, 250
- Masters K. L., et al., 2019, *MNRAS*, **487**, 1808
- Moresco M., et al., 2013, *A&A*, **558**, A61
- Mortlock A., et al., 2013, *MNRAS*, **433**, 1185
- Muzzin A., et al., 2013, *ApJ*, **777**, 18
- Naim A., et al., 1995, *MNRAS*, **274**, 1107
- Nair P. B., Abraham R. G., 2010, *ApJS*, **186**, 427
- Osterbrock D. E., Ferland G. J., 2006, *Astrophysics of gaseous nebulae and active galactic nuclei*. University Science Books
- Panter B., Heavens A. F., Jimenez R., 2003, *MNRAS*, **343**, 1145
- Panter B., Jimenez R., Heavens A. F., Charlot S., 2007, *MNRAS*, **378**, 1550
- Peng Y.-j., et al., 2010, *ApJ*, **721**, 193
- Pérez E., et al., 2013, *ApJ*, **764**, L1
- Peterken T. G., et al., 2019, *MNRAS*, **489**, 1338
- Peterken T., Merrifield M., Aragón-Salamanca A., Fraser-McKelvie A., Avila-Reese V., Riffel R., Knapen J., Drory N., 2020, *MNRAS*, **495**, 3387
- Peterken T., Merrifield M., Aragón-Salamanca A., Avila-Reese V., Boardman N. F., Drory N., Lane R. R., 2021, *MNRAS*, **500**, L42
- Pfarr J., Maraston C., Tonini C., 2012, *MNRAS*, **422**, 3285
- Planck Collaboration et al., 2016, *A&A*, **594**, A13
- Roberts M. S., 1963, *ARA&A*, **1**, 149
- Rodríguez-Puebla A., Calette A. R., Avila-Reese V., Rodríguez-Gomez V., Huertas-Company M., 2020, arXiv e-prints, p. arXiv:2004.13740
- Sánchez S. F., et al., 2016, *Rev. Mex. Astron. Astrofis.*, **52**, 21
- Sánchez S. F., et al., 2019, *MNRAS*, **482**, 1557
- Schawinski K., et al., 2014, *MNRAS*, **440**, 889
- Smee S. A., et al., 2013, *AJ*, **146**, 32
- Smethurst R. J., et al., 2015, *MNRAS*, **450**, 435
- Smethurst R. J., Lintott C. J., Bamford S. P., Hart R. E., Kruk S. J., Masters K. L., Nichol R. C., Simmons B. D., 2017, *MNRAS*, **469**, 3670
- Smethurst R. J., et al., 2018, *MNRAS*, **473**, 2679
- Vazdekis A., Koleva M., Ricciardelli E., Röck B., Falcón-Barroso J., 2016, *MNRAS*, **463**, 3409
- Wake D. A., et al., 2017, *AJ*, **154**, 86
- Wang B., Cappellari M., Peng Y., Graham M., 2020, *MNRAS*, **495**, 1958
- Westfall K. B., et al., 2019, *AJ*, **158**, 231
- Willett K. W., et al., 2013, *MNRAS*, **435**, 2835
- Wuyts S., et al., 2011, *ApJ*, **742**, 96
- Yan R., et al., 2016a, *AJ*, **151**, 8
- Yan R., et al., 2016b, *AJ*, **152**, 197
- Yi S. K., 2003, *ApJ*, **582**, 202
- Yi S. K., 2008, in Heber U., Jeffery C. S., Napiwotzki R., eds, *Astronomical Society of the Pacific Conference Series Vol. 392, Hot Subdwarf Stars and Related Objects*. Astronomical Society of the Pacific, p. 3
- de Amorim A. L., et al., 2017, *MNRAS*, **471**, 3727
- van Dokkum P. G., et al., 2008, *ApJ*, **677**, L5

This paper has been typeset from a $\text{\TeX}/\text{\LaTeX}$ file prepared by the author.